Lagrangian Eddy Scales in the Northern Atlantic Ocean

RICK LUMPKIN

Department of Oceanography, The Florida State University, Tallahassee, Florida, and Laboratoire de Physique des Océans, IFREMER, CNRS, Plouzane, France

ANNE-MARIE TREGUIER

Laboratoire de Physique des Océans, IFREMER, CNRS, Plouzane, France

KEVIN SPEER

Department of Oceanography, The Florida State University, Tallahassee, Florida

(Manuscript received 12 April 2000, in final form 3 December 2001)

ABSTRACT

Eddy time and length scales are calculated from surface drifter and subsurface float observations in the northern Atlantic Ocean. Outside the energetic Gulf Stream, subsurface timescales are relatively constant at depths from 700 m to 2000 m. Length scale and the characteristic eddy speed decrease with increasing depth below 700 m, but length scale stays relatively constant in the upper several hundred meters of the Gulf Stream. It is suggested that this behavior is due to the Lagrangian sampling of the mesoscale field, in limits set by the Eulerian eddy scales and the eddy kinetic energy. In high-energy regions of the surface and near-surface North Atlantic, the eddy field is in the ''frozen field'' Lagrangian sampling regime for which the Lagrangian and Eulerian *length* scales are proportional. However, throughout much of the deep ocean interior, the eddy field may be in the ''fixed float'' regime for which the Lagrangian and Eulerian *time*scales are nearly equal. This does not necessarily imply that the deep interior is nearly linear, as fixed-float sampling is possible in a flow field of $O(1)$ nonlinearity.

1. Introduction

In this paper, we present and interpret the distribution of Lagrangian eddy scales measured by drifters and floats in the Northern Hemisphere of the Atlantic Ocean. In recent years, the density of subsurface drifter observations has grown considerably, allowing far greater resolution of Lagrangian scale vertical distribution than previously published (Böning 1988). We also examine simulated drifters in a $\frac{1}{3}°$ eddy-permitting primitive equation model of the Atlantic, to help understand why the scales have their observed distribution.

We must first define ''Lagrangian eddy scales.'' Consider a particle released into a fluid that subsequently moves at speed $U(t)$. This speed can be divided into a mean component U_o, which is the same for all particles passing through a fixed point (at any time), and a time-varying component $u(t)$, which varies from particle to particle. For a spatially homogeneous U_o, the position of the particle is $X(t) = U_o t + x(t)$, where

$$x(t) = \int_0^t d\tau u(\tau). \qquad (1)$$

Assuming that u is ergodic, (1) can be used to derive Taylor's Theorem (Taylor 1921):

$$\langle x^2 \rangle = 2u'^2 \int_0^t d\tau (t - \tau) R(\tau), \qquad (2)$$

where the dispersion $\langle x^2 \rangle$ is an average over many particles of x^2, u' is the characteristic eddy speed given by the standard deviation of u, and the velocity autocorrelation R is

$$R(\tau) = \lim_{T_m \to \infty} \frac{1}{u'^2 T_m} \int_0^{T_m} dt u(t) u(t + \tau). \qquad (3)$$

The characteristic timescale of dispersion is the Lagrangian eddy timescale T_L,

$$T_L = \int_0^\infty d\tau R. \qquad (4)$$

This is the lag over which a particle's speed stays strongly correlated with itself. Because the particle moves at

Corresponding author address: Rick Lumpkin, Dept. of Oceanography, The Florida State University, Tallahassee, FL 32306-4320.
E-mail: rlumpkin@ocean.fsu.edu

a characteristic speed u', this timescale corresponds to a distance

$$L_L = u'T_L \tag{5}$$

called the Lagrangian eddy length scale. By analogy with Fickian diffusion, $\langle x^2 \rangle$ can be related to an effective eddy diffusivity

$$\kappa_H = \frac{1}{2}\frac{d}{dt}\langle x^2 \rangle \tag{6}$$

(Taylor 1921; Batchelor 1949), which asymptotes to

$$\kappa_H = u'L_L \tag{7}$$

in the random-walk limit $t \gg T_L$ (cf. Davis 1982, Garrett 1994).

Early efforts to map κ_H from float observations in MODE (depth 1500 m) and LDE (700 m, 1400 m) found a diffusivity that varied with u'^2, consistent with an approximately constant timescale $T_L \sim 7–9$ days (Price, in Rossby et al. 1983 and McWilliams et al. 1983). Poulain and Niiler (1989) found a similar relationship for κ_H in the California Current System, but with a much shorter timescale (4.1–4.9 d). If a constant-T_L rule (or, alternatively, a constant-L_L rule) were universal, it would be of tremendous value: maps of κ_H could be estimated directly from the distribution of EKE (Böning 1988). However, subsequent studies found that a constant-T_L rule did not apply elsewhere. For near-surface drifters in the North Atlantic, diffusivity varied with u', suggesting a constant length scale $L_L \sim 31–39$ km (Krauss and Böning 1987). Brink et al. (1991) found a similar relationship (with $L_L = 42$ km) for surface drifters in the California coastal transition zone, an energetic near-coast subset of the Poulain and Niiler (1989) study region. Böning (1988) used float observations at various depths to estimate the vertical distribution of T_L and L_L in the North Atlantic, and suggested that the floats encountered a depth-dependent, but u'-independent, L_L (i.e., $T_L \propto 1/u'$). Numerical simulations conducted by Hua et al. (1998) are also consistent with near-constant L_L. More recent drifter studies (Swenson and Niiler 1996; Lumpkin and Flament 2001) have found both L_L and T_L to vary with u' over large regions of the ocean surface. Clearly, neither a constant-T_L nor a constant-L_L rule is universal—but what are the dynamics that make them regionally applicable? Can we anticipate such rules in other regions of the ocean?

In the following sections, we present the observations used in this study (section 2), describe how eddy scales were calculated (section 3), and present the observed distribution of scales in the northern Atlantic (section 4). We then address why this distribution is observed by reviewing the relationship between Lagrangian and Eulerian scales (section 5) and examining the distribution of these scales in an eddy-permitting model (section 6). We speculate how these results may extend to the real ocean (section 7) and summarize our conclusions (section 8). In two appendices, we discuss alternative methods of calculating Lagrangian scales and discuss sources of scatter when comparing Lagrangian and Eulerian scales in the numerical model.

2. Data

Northern Atlantic surface drifter trajectories for 1989–97 were obtained from the Marine Environmental Data Service. The drifters were standard WOCE/SVP drifters (Niiler et al. 1987) with a holey-sock drogue centered at depth 15 m. A two-step quality evaluation algorithm was used to eliminate errors in the raw fixes, which were then interpolating to 1-day intervals via kriging (Hansen and Poulain 1996). The interpolated data spanned 738 drifter-years, with most observations concentrated between 25° and 40°N (Fig. 1). An important caveat of these drifters is that they follow the total (geostrophic and ageostrophic) near-surface flow, including Ekman drift. In regions where the wind-forced drift contributes significantly to eddy energy, Lagrangian scales derived from the total motion will be smaller than those derived from the geostrophic component alone. This effect should be least significant in currents such as the Gulf Stream and North Atlantic Current, where intense eddies and geostrophic mean flow dominate drifter motion. Farther north, where geostrophic eddy energy is weaker and winter storms can be intense, this effect may be pronounced.

Subsurface (SOFAR, RAFOS, and MARVOR) float trajectories were compiled from experiments in the tropical and northern Atlantic,[1] including two years of Eurofloats deployed in the deep northeastern Atlantic (Speer et al. 1999). A total of 588 float years were collected, spanning over 24 years from 1973 to 1998; 75% of observations deeper than 1000 m were made after 1985. The floats were at 90–4100 m, with half the observations concentrated in three narrow depth bins: 600–800 m (22% of data), 1000–1200 m (13%), and 1700–1900 m (15%).

3. Calculating eddy scales

Lagrangian scales were calculated from nonoverlapping 120-day segments of the float trajectories. Time series of zonal (u_1) and meridional (u_2) speeds were calculated for each trajectory segment via finite differencing. The mean and linear trend in the u_i were removed in order to minimize artificial magnification of the Lagrangian scales by shear in the pseudo-Eulerian mean flow field (cf. Krauss and Böning 1987). The autocorrelation functions R_{ii} were calculated using (3), with $T_m = 120$ days. Because noise tends to dominate R for large lags, we followed the standard practice (cf. Freeland et al. 1975; Krauss and Böning 1987; Poulain and Niiler 1989) of integrating (4) to the first zero crossing.

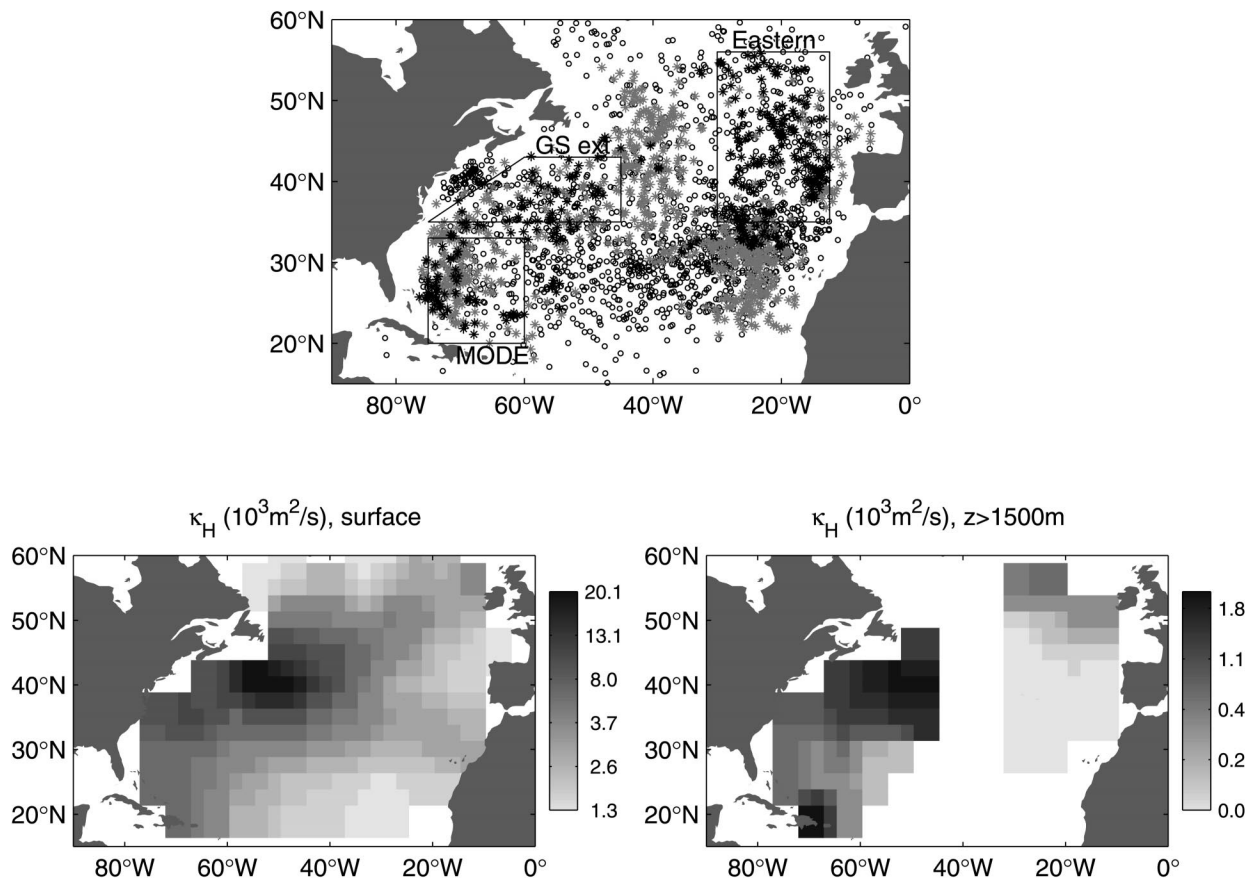[1] For a tabulation of these data, see O'Dwyer et al. (2000).

FIG. 1. (Top) median positions for 120-day segments of drifter and float trajectories at the surface (open circles), subsurface to depth 1500 m (gray stars), and deeper than 1500 m (black stars). Boxes indicate regions isolated in Fig. 3. Bottom: apparent eddy diffusivity from surface drifters (left) and floats below 1500 m (right).

These approximations to Eqs. (3) and (4) allow the maximum amount of data to be used in mapping the Lagrangian scales, but one should be aware of their effects. By removing the mean and linear trend of each 120-day segment, we discard low-frequency variability as well as the spatially varying mean field. With heavy sampling, such as in a regional deployment of a float cluster at one depth, one would prefer removing a time-mean flow, obtained by pseudo-Eulerian averaging of the floats and interpolated onto the individual trajectories. However, throughout much of the Atlantic, the full three-dimensional pseudo-Eulerian mean field is poorly resolved by the floats at scales finer than several degrees. By neglecting low-frequency variability, the scales T_L and L_L are artificially shortened. In contrast, truncating the integral in (4) at the first zero crossing of R tends to magnify T_L and L_L because R may have a prominent negative lobe beyond that crossing. In appendix A, we examine this second approximation by comparing alternative methods for approximating (4).

Horizontal averages (and their standard errors) of the eddy scales were calculated in 10° cells. Lagrangian scales from each 120-day trajectory were treated as point measurements located at the trajectory's median

longitude and latitude. Averages were not calculated where less than 10 estimates were obtained. Over 120 days, the average 1750-m-deep float traveled 150 km; 1.4% of the floats traveled over 1000 km in 120 days. The average surface drifter traveled 380 km in 120 days, and 14% traveled over 1000 km (2% experienced persistent mean currents greater than 20 cm s^{-1} over 120 days, thus traveling over 2000 km). We retained the trajectories spanning more than 10° in the averaging, although at least a small fraction of each consists of observations in neighboring cells; rejecting these trajectories would have biased the averages toward times of weak currents. As a consequence of retaining long trajectories, surface maps of the Lagrangian eddy scales may be ''smoothed'' along the direction of strong mean currents. In these maps, we shall present the average of the zonal and meridional components: $u' = 0.5 \Sigma_i u_i'$, $T_L = 0.5 \Sigma_i T_{L,i}$, $L_L = 0.5 \Sigma_i L_{L,i}$.

Maps of the scales' horizontal distribution shall be presented in two layers: surface (i.e., the near-surface WOCE drifters) and ''deep,'' the latter layer encompassing all floats between 1700 and 2000 m. We focus upon these two layers as they present well-sampled extremes in the oceanic EKE level. Observations at all
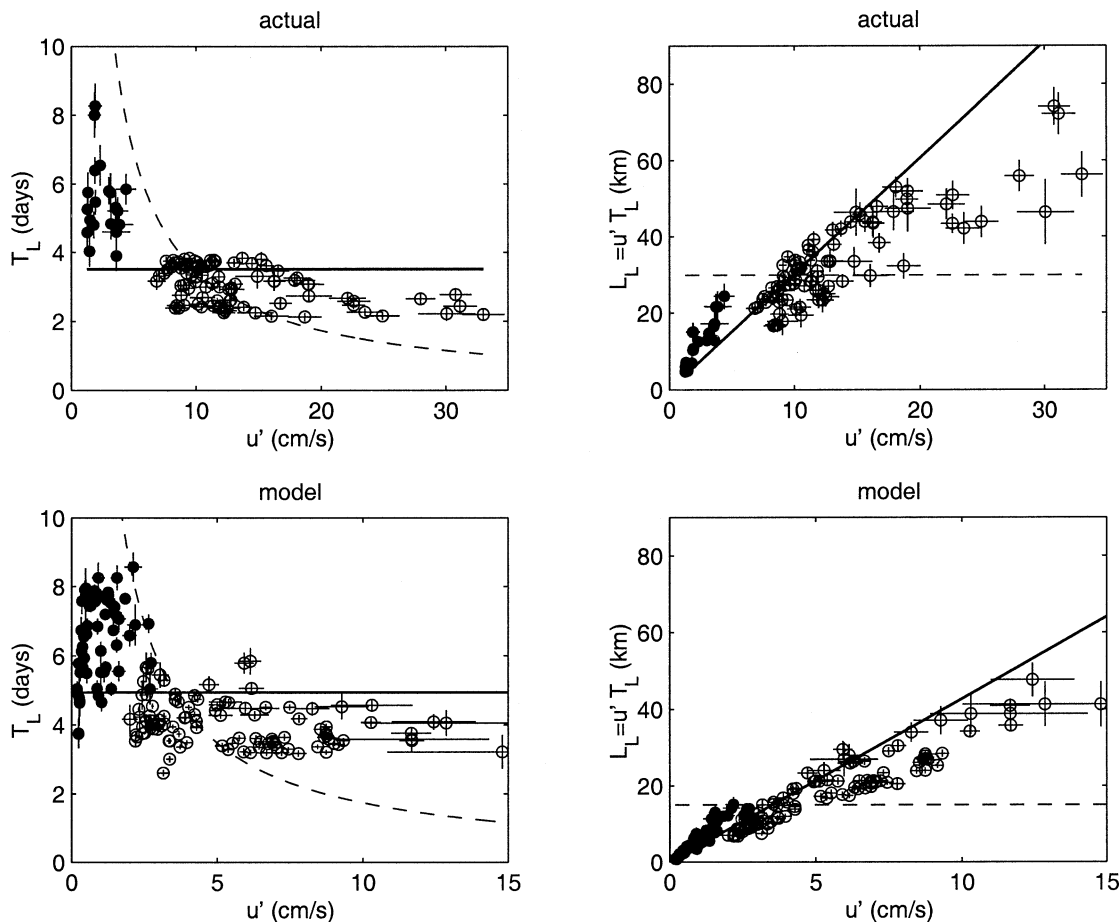
FIG. 2. Lagrangian time (left) and length (right) eddy scales vs eddy speed, for actual (top) and simulated (bottom) float trajectories. Open circles are at the surface, filled points are in the deep layer (1700–2000 m). The scales have been averaged in 10° cells; standard error bars (thin lines) are calculated from the scatter of values within each cell. Heavy solid lines show the distributions if T_L were constant everywhere (the overall mean is used). Dashed lines show the distributions if $u'T_L = L_L$ were constant everywhere (the overall mean of L_L is used).

depths were used to calculate the various scales' vertical distributions.

4. Observations

Figure 1 shows the apparent eddy diffusivity κ_H calculated via (7) for surface drifters and for floats deeper than 1500 m. Surface values of κ_H are nearly an order of magnitude larger than the deep values, reflecting the larger eddy energy and Lagrangian length scales at the surface. In both layers, the largest values are found in the western Atlantic. Surface values peak in the Gulf Stream extension, where the maximum value of $22.8 \pm 1.8 \times 10^3$ m^2 s^{-1} is found in the cell south of the Grand Banks. Regional surface maxima in κ_H extend along the path of the North Atlantic Current and the Azores Current (cf. Fratantoni 2001). Deep values are largest along the path of the deep western boundary current, and extremely small values of κ_H, averaging 70 ± 10 m^2 s^{-1}, are found in the deep eastern Atlantic south of 50°N.

Figure 2 (top panels) shows T_L and L_L versus u' in the surface and deep layers of the northern Atlantic. The general tendency is for T_L to decrease, and L_L to increase, with increasing u', as found in recent large-scale drifter studies (Swenson and Niiler 1996; Lumpkin and Flament 2001). Unlike in the regional studies discussed earlier, neither a constant-T_L or constant-L_L "rule" characterizes the full set of observations.

Deep float observations are concentrated in three regions (see Fig. 1): the Gulf Stream extension region (Owens 1991), the MODE region (Freeland et al. 1975; Rossby et al. 1983) (as defined here, a much broader region than that of MODE which encompasses the southwestern subtropics), and the eastern basin region of Eurofloat and ARCANE deployments (Speer et al. 1999). Vertical distributions of the Lagrangian scales in these regions are shown in Fig. 3 (which may be compared with Böning 1988, Fig. 2).

In all three regions, u' decreases by 2–2.5 times between the surface and 700–1000 m, and 1.5–2 times
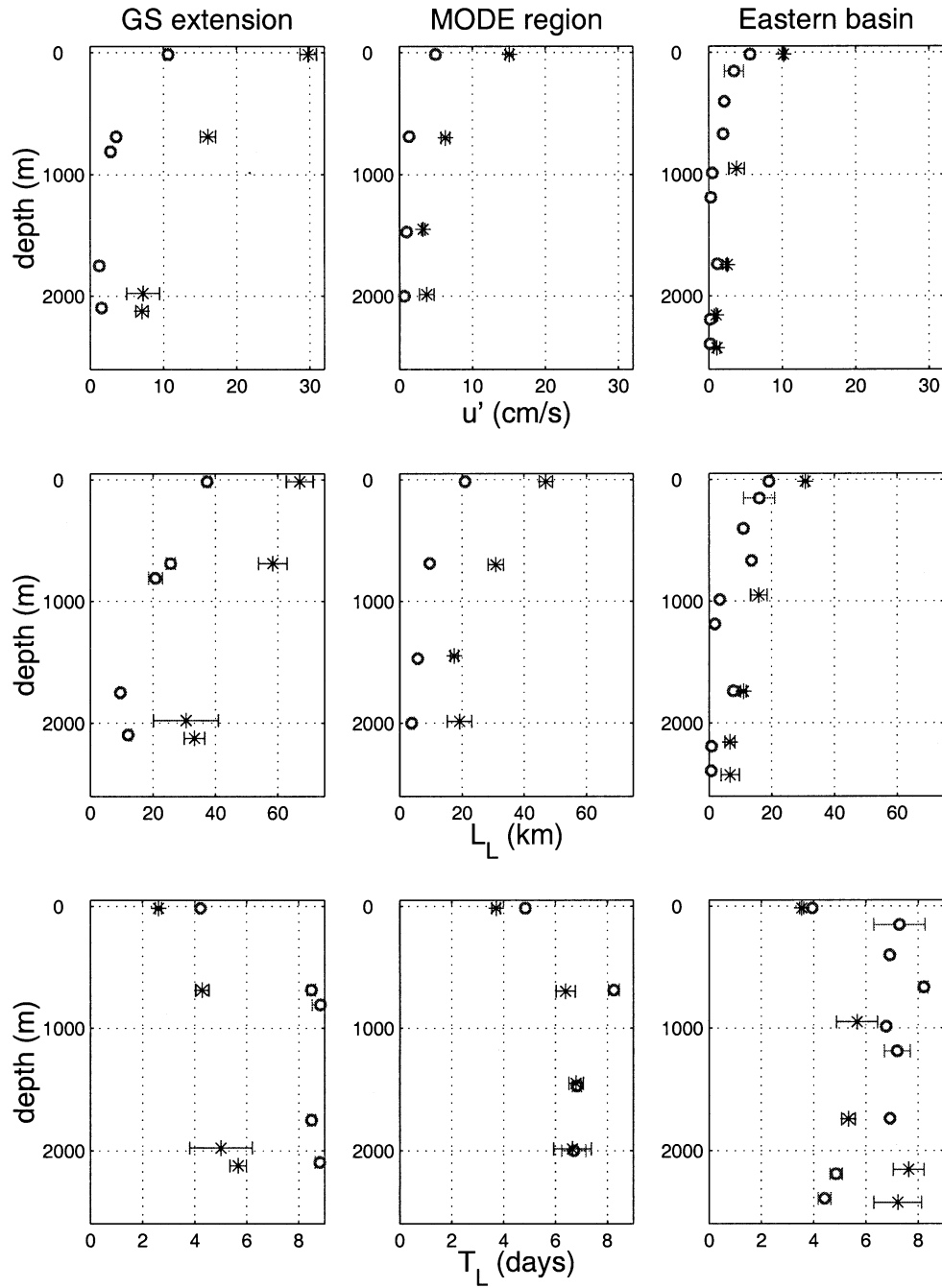
FIG. 3. Lagrangian eddy speed (top) and length (middle) and time (bottom) scales as a function of depth for the actual (asterisks) and simulated (circles) floats. Each column corresponds to a region shown in Fig. 1. Standard error bars are indicated.

between 700 and 2000 m. In the "MODE" and "Eastern" basin regions, L_L has similar profiles. In the energetic Gulf Stream region, L_L decays by a barely significant 1.2 times (from 67 to 57 km) between the surface and 700 m. In all three regions, timescale T_L increases by 1.5–1.7 times between the surface and depth 700–1000 m; in the MODE and Eastern regions, T_L remains approximately constant (5.3–6.6 days) below

700 m, with the only significant change in subsurface $T_L(z)$ between 1750 and 2150 m in the Eastern basin. In the Gulf Stream region, T_L is small (4.2 days) at 700 m, and increases a significant 1.3 times between 700 and 2150 m.

Figure 4 shows the horizontal distribution of Lagrangian eddy scales. At the surface, T_L reaches its largest values (~4 days) in the center of the subtropical
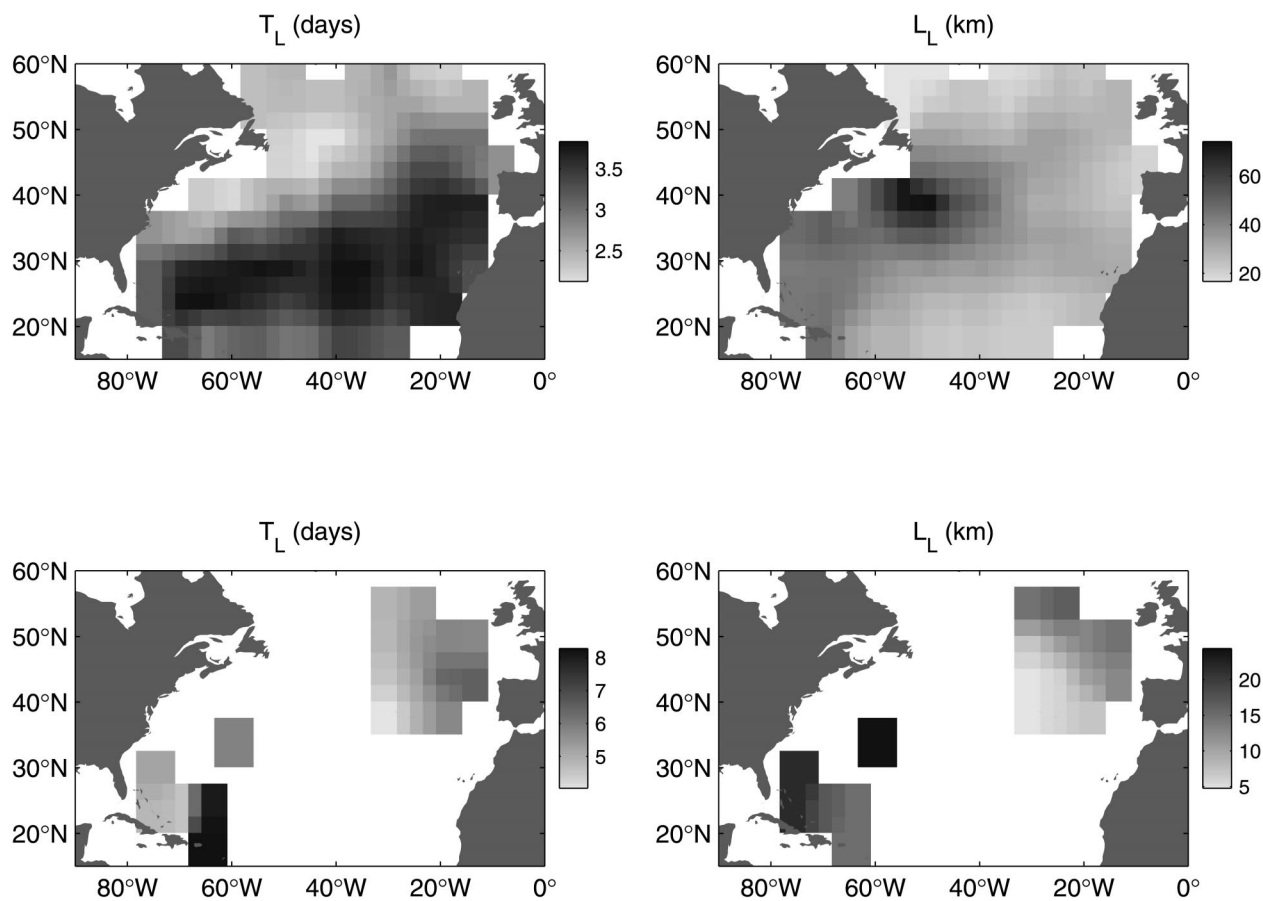
FIG. 4. Lagrangian eddy scales observed by surface (top) and deep (bottom) drifters and floats. The time (left) and length (right) scales have been averaged in 10° cells.

gyre and drops to smaller values in the far northern Atlantic. Surface L_L ($=u'T_L$) reaches maximum values of ~70 km in the Gulf Stream. In the deep layer, T_L is smallest (4–6 days) in the eastern basin, and reaches maxima of ~9 days in the Tropics. Deep L_L are 5–20 km, much smaller than at the surface.

At the surface, maxima in zonally averaged u' (Fig. 5) correspond to the locations of major currents (Gulf Stream, North Atlantic Current, and possibly the Azores Current), suggesting eddy generation by baroclinic instability (Stammer 1997, 1998). Peaks in zonally averaged L_L (Fig. 6) generally correspond to those in u' for both surface and deep observations. Variations in zonally averaged T_L (Fig. 7) show the surface maximum at 30°N.

5. Relating Lagrangian and Eulerian scales

As a float passes through an eddy field, it mixes the field's spatial and temporal variability in its time series of displacement. The resulting relationship between T_L and T_E was quantified by Middleton (1985) for an idealized 2D, nondivergent, homogeneous, stationary eddy field. Middleton assumed Corrsin's (1950) conjecture

and Gaussian mean-square Lagrangian displacements (the "parameterized Gaussian model" of Davis 1982). He found that the ratio T_L/T_E depends on the parameter u'/c_* (his α, Davis' τ_M/τ_E), where u' is the rms eddy speed and

$$c_* \equiv L_E/T_E \qquad (8)$$

is the *evolution speed* of the eddy field, constructed from its Eulerian time and length scales. Middleton considered a wide range of possible statistics for the Eulerian field and showed that T_L/T_E could be predicted to within ~10% by

$$T_L/T_E = q[q^2 + (u'/c_*)^2]^{-1/2}, \qquad (9)$$

where $q = \sqrt{\pi/8}$. Using the definition of L_L,

$$L_L/L_E = (u'/c_*)[1 + (u'/c_*q)^2]^{-1/2}. \qquad (10)$$

To visualize why the scales should be related according to (9) and (10), consider the two extremes of the Lagrangian sampling regime parameter u'/c_*. If $u'/c_* < 1/2$, a float travels a fraction of L_E before the current has changed substantially due to temporal fluctuations, so $L_L < 0.4L_E$. In this *fixed-float* regime, the float samples mesoscale fluctuations like a fixed current meter
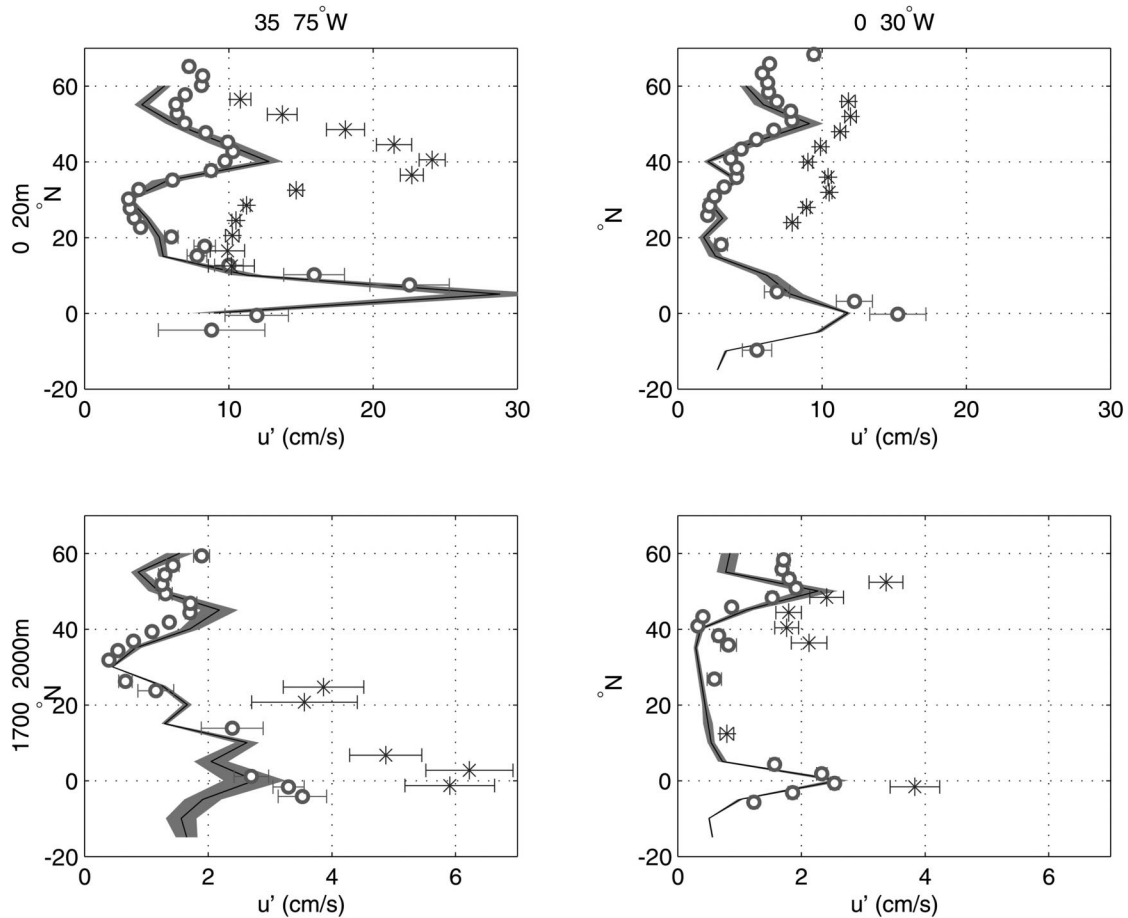
FIG. 5. Lagrangian eddy speed u' as a function of latitude for the actual (asterisks) and simulated (circles) floats, with standard error bars. The zonal averages are conducted separately for surface (top) and deep (bottom) observations and data west of 35°W (left) and east of 30°W (right). Solid lines with shaded error bars indicate zonally averaged u' from the high-passed model output, weighted by the mean density of simulated Lagrangian observations.

on a mooring: $T_L \sim T_E$. [Of course, because the float is not truly fixed, current meter and float time series of $u(t)$ will diverge for $t \gg T_L$.] At the other extreme $u'/c_* > 1$ [characterizing the Davis (1985) CODE observations], a float travels across many eddies before the field evolves significantly, so $T_L < 0.5T_E$. In this *frozen-field* regime, $L_L \propto L_E$ because the eddy size determines the radii of curvature in the float trajectory's meanders. At intermediate values $1/2 < u'/c_* < 1$, both temporal and spatial variations of the Eulerian field play a lowest-order role in determining the Lagrangian scales.

6. Lagrangian and Eulerian scales in CLIPPER

In order to directly compare Eulerian and Lagrangian scales throughout the ocean, float observations were simulated in the CLIPPER North Atlantic primitive equation model (Treguier et al. 1999, 2001). The model uses an isotropic Mercator C-grid of ⅓° resolution at the equator with a corresponding grid size ranging from

37 km (equator) to 12.6 km (70°N). It has 42 vertical layers extending to a maximum depth of 5500 m with spacing increasing smoothly from 12 m (surface) to 200 m (below 1000 m). The model domain is 75°S–70°N, 98.5°W–20°E. In the North Atlantic, its configuration closely resembles that of the WOCE Community Modeling Effort (CME) ⅓° simulation. In the CME model, the eddy field is weaker than in the real ocean, but the model replicates the altimeter-observed poleward decrease in Eulerian length scale (Stammer and Böning 1992).

The model was spun up for 8 years using the monthly means of the ECMWF climatology (years 79–93), then run for those individual years using daily forcing. Model currents during years 84–88 were integrated using the interpolation technique of Blanke and Raynaud (1997) to produce continuous trajectories for 2480 simulated isobaric Lagrangian floats, at depths from the surface to 4080 m. The simulated floats were "released" at the deployment locations of the actual floats, and Lagrangian eddy scales were calculated from their trajectories
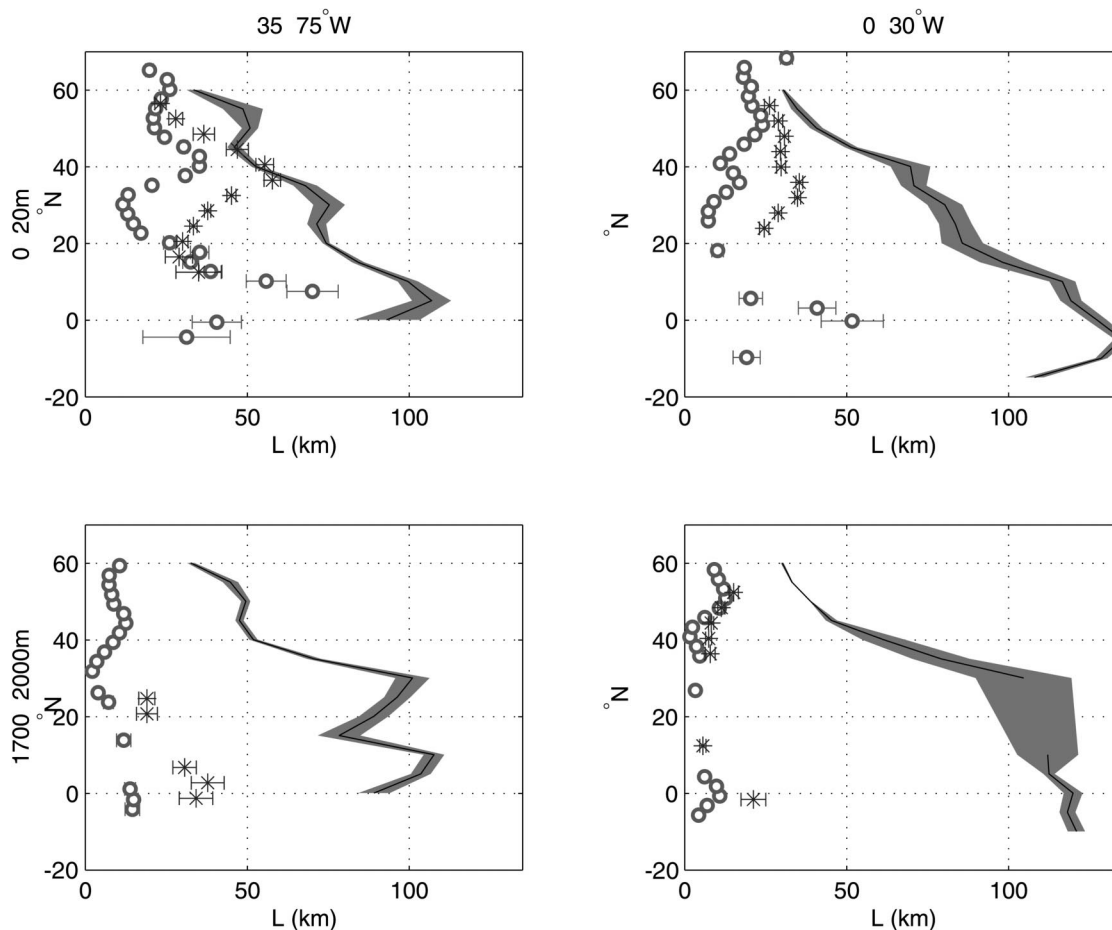
Fig. 6. Lagrangian length scale L_L as a function of latitude for the actual (asterisks) and simulated (circles) floats, with standard error bars. The zonal averages are conducted separately for surface (top) and deep (bottom) observations and data west of 35°W (left) and east of 30°W (right). Solid lines with shaded error bars indicate zonally averaged L_E calculated from the high-passed model output, multiplied by $q = \sqrt{\pi/8} \sim 0.63$ and weighted by the mean density of simulated Lagrangian observations.

as done with the actual floats. Because the simulated drifters and floats never died, they sampled the model ocean more densely than done by the actual drifter/ floats.

Eulerian eddy scales were calculated from the model currents during the four years of float simulation. The currents were stored every 4 days at 1° resolution and broken into 120-day segments, each yielding an estimate of T_E (calculated as with T_L). Eulerian length scale L_E was calculated from monthly current snapshots at the full model resolution. The currents were high passed at 150 days to isolate the eddy field (Stammer and Böning 1992). Spatial autocorrelation functions of the u_i were calculated in 10° cells on a grid with 5° overlap (every other cell was independent). These autocorrelation functions were spatially integrated to their first zero crossing and multiplied by two, for consistency with the decorrelation scale L_E of Middleton (1985).

When presenting Eulerian eddy scales from the mod-

el, the "surface layer" is the uppermost model layer and the "deep layer" is the model layer at 1806 m.

Simulated scales in the model

Figure 2 (bottom) shows T_L and L_L versus u' in the model. Simulated u' are smaller than those observed in the actual ocean by 2–3 times, due to the ⅓° model resolution (Stammer and Böning 1992). Simulated L_L are also smaller than in the actual ocean.[2] However, the distributions of actual and simulated u' and L_L have similar distributions to those in the real ocean (Figs. 3, 5, 6). Simulated and actual T_L have similar values in the quieter MODE and Eastern basin regions, but sim-

---

[2] Simulated length scales much smaller than ⅓° in a ⅓° model may seem paradoxical, but are not: float displacements by the interpolated velocity field can be subgrid scale in the fixed-float regime. Eulerian scales, on the other hand, cannot be (and are not) subgrid scale.
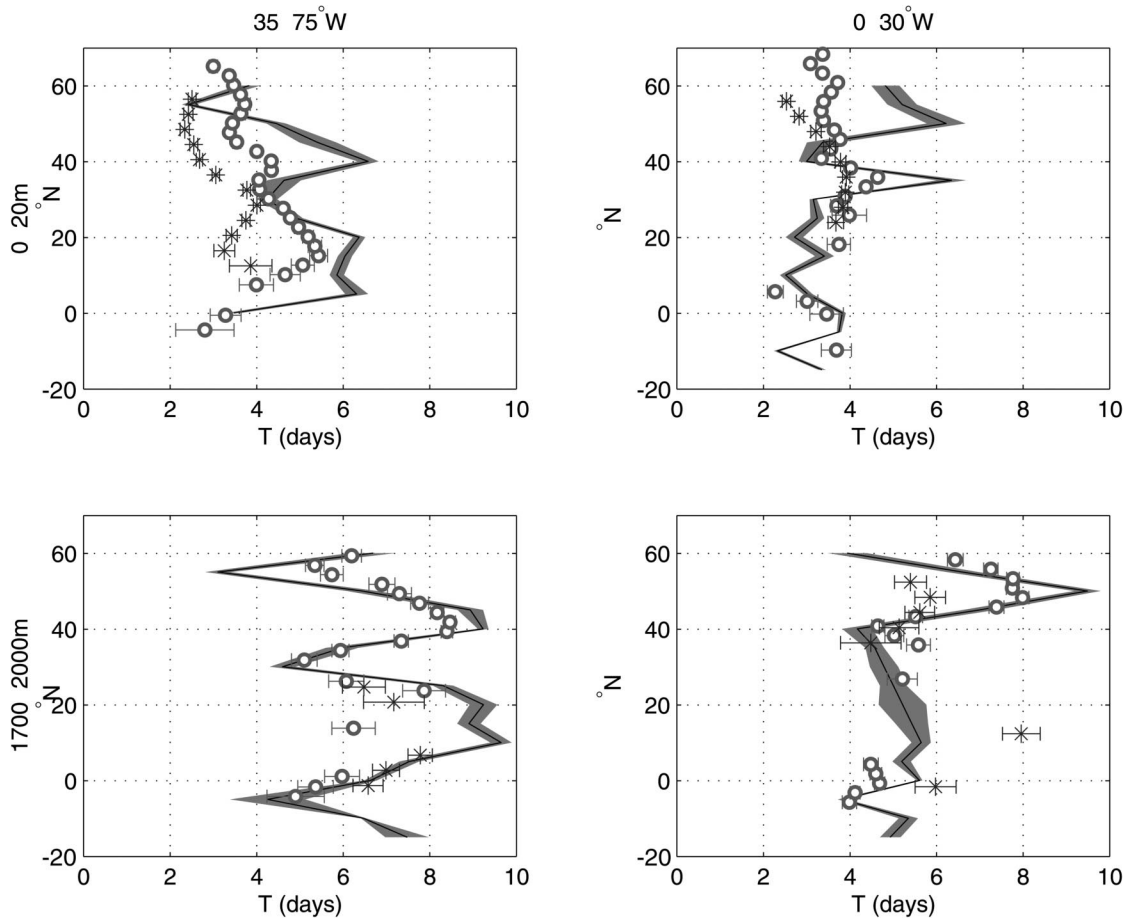
FIG. 7. Lagrangian timescale T_L as a function of latitude for the actual (stars) and simulated (circles) floats, with standard error bars. The zonal averages are conducted separately for surface (top) and deep (bottom) observations and data west of 35°W (left) and east of 30°W (right). Solid lines with shaded error bars indicate zonally averaged T_E calculated from the high-passed model output, weighted by the mean density of simulated Lagrangian observations.

ulated T_L are consistently larger (by 1.6–2 times below the surface) in the Gulf Stream region.

Simulated L_E decreases with increasing latitude, as in the CME model and in altimetric observations (Stammer and Böning 1992; Stammer 1997). The distribution of simulated $L_L = u'T_L$ is completely different, primarily mirroring the distribution of u'. In contrast, simulated T_E and T_L are distributed similarly, particularly in the deep layer.

Figure 8 compares the Lagrangian and Eulerian scales in the model. In the deep layer, $T_L \sim T_E$ and there is no apparent relationship between L_L and L_E. The maximum value of u'/c_* is 0.25, and L_L/L_E grows linearly with increasing u'/c_*. In the surface layer, u'/c_* exceeds unity in some 10° cells. In these high-energy cells, T_L/T_E drops to 0.5. The linear growth of L_L/L_E at small u'/c_* does not persist for $u'/c_* > 0.5$.

7. Discussion

In the model, T_L/T_E and L_L/L_E vary with the non-dimensional sampling parameter u'/c_* approximately

as predicted by (9) and (10), although the 10° averages do not fall precisely on the predicted curves (see appendix B). We conclude that the relationship of Middleton (1985) approximately describes the relationships between Lagrangian and Eulerian scales in the primitive equation model, and by extension may apply to the real ocean (at least over the simulated range of u'/c_*).

a. The ocean's sampling regimes

In the model, most of the surface drifters experience fixed-float conditions—the overall median u'/c_* is 0.23 (Fig. 8). In the most energetic 10° cells, drifters experience intermediate to frozen-field values of u'/c_*: along the simulated North Atlantic current, $u'/c_* \sim 0.6$–1; in two Gulf Stream cells, $u'/c_* > 1.2$. The deep model layer is entirely within the fixed-float regime: maximum values of u'/c_* are ~ 0.2, $T_L \sim T_E$ in all 10° cells, and L_L/L_E increases linearly with u'/c_*.
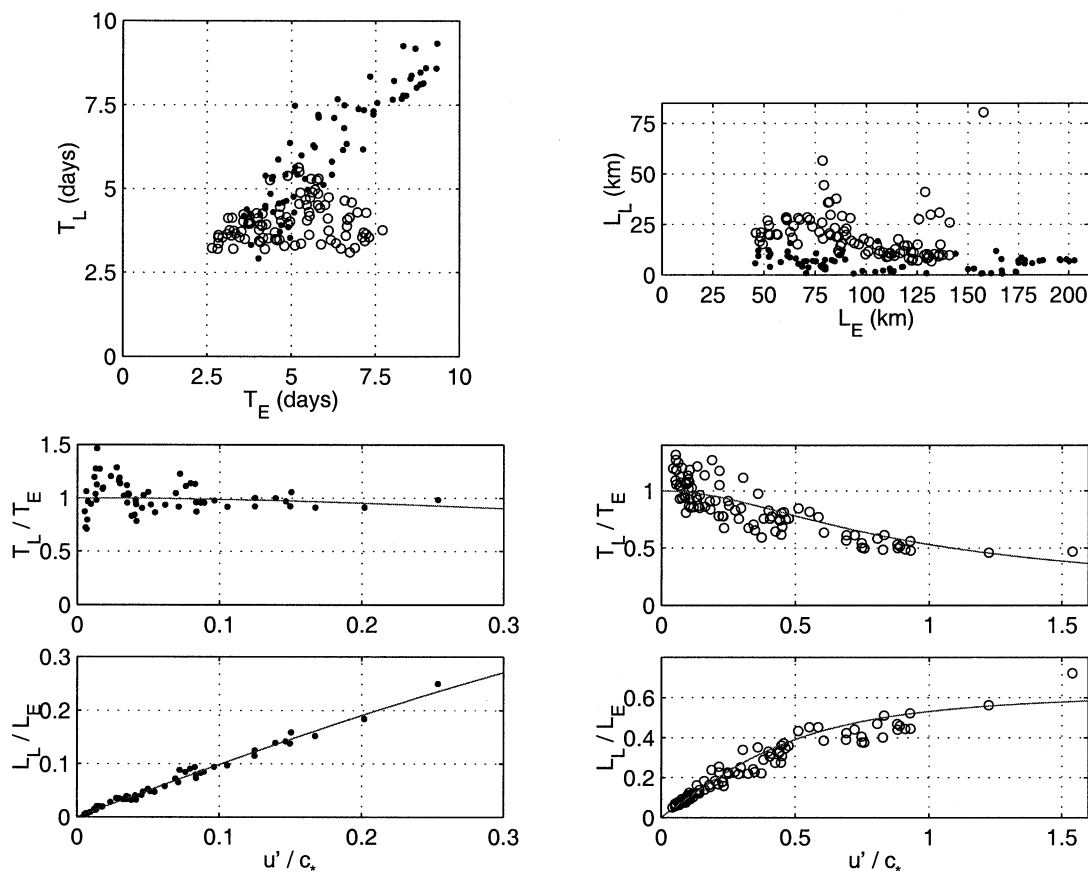
What sampling regime do actual surface drifters ex-

FIG. 8. A comparison of Lagrangian and Eulerian scales in the surface (open circles) and deep (filled points) layers of the model. Each point is a 10° average. Top Lagrangian time (left) and length (right) scales vs their Eulerian counterparts. Bottom ratio of Lagrangian to Eulerian length (left) and time (right) scales vs the sampling regime parameter u'/c. Solid lines show the theoretical ratio (Middleton 1985).

perience? A direct estimate of surface u'/c_* can be made from drifter-derived u' and altimetry-derived T_E and L_E (Stammer 1997; his Figs. 18b and 21a). This estimate (Fig. 9) suggests that more than half the 10° cells have $u'/c_* < 1$, with 10% in the fixed-float range $u'/c_* < 1/2$. Frozen-field values ($u'/c_* > 1$) are found along the Gulf Stream, Gulf Stream extension, and North Atlantic Current. Despite potential inconsistencies between definitions of Eulerian scales in Middleton (1985) and Stammer (1997), and contamination by Ekman motion, the ratio of Lagrangian to Eulerian scales are not grossly different from those predicted by Middleton's theory: maximum L_L/L_E and minimum T_L/T_E fall in the Gulf Stream extension, where u'/c_* reaches its maximum of 2.4. Minimum L_L/L_E and maximum T_L/T_E coincide with fixed-float (<1/2) values of u'/c_*.

The deep distribution of Eulerian scales remains unknown, although there are point estimates of T_E from current meter moorings. In MODE, the Eulerian and Lagrangian timescales were nearly equal (Freeland et al. 1975), consistent with the fixed-float sampling hypothesis. As future concurrent Lagrangian and Eulerian

measurements are made, the generality of this behavior should be examined.

b. Implications for simple empirical rules

If the sampling regime of the mesoscale eddy field varies from frozen field to fixed float, there will be regions described by a nearly constant T_L or L_L, as found in previous studies. To demonstrate this, suppose that float observations are collected over a region where the Eulerian scales T_E and L_E are nearly constant but the eddy kinetic energy level varies. If $u'/c_* > 1$ throughout the region, it is in the frozen-field regime where $L_L = qL_E$ and $T_L \propto 1/u'$—there will be a nearly constant Lagrangian length scale L_L, as found in the near-surface North Atlantic (Krauss and Böning 1987). However, if $u'/c_* < 1/2$, the field is in the fixed-float regime where $T_L \approx T_E$ and $L_L \propto u'$—there will be a nearly constant timescale T_L, as in the MODE and LDE regions (Rossby et al. 1983; McWilliams et al. 1983). If the field is intermediate, both T_L and L_L will vary with u'. This interpretation is consistent with the numerical simula-
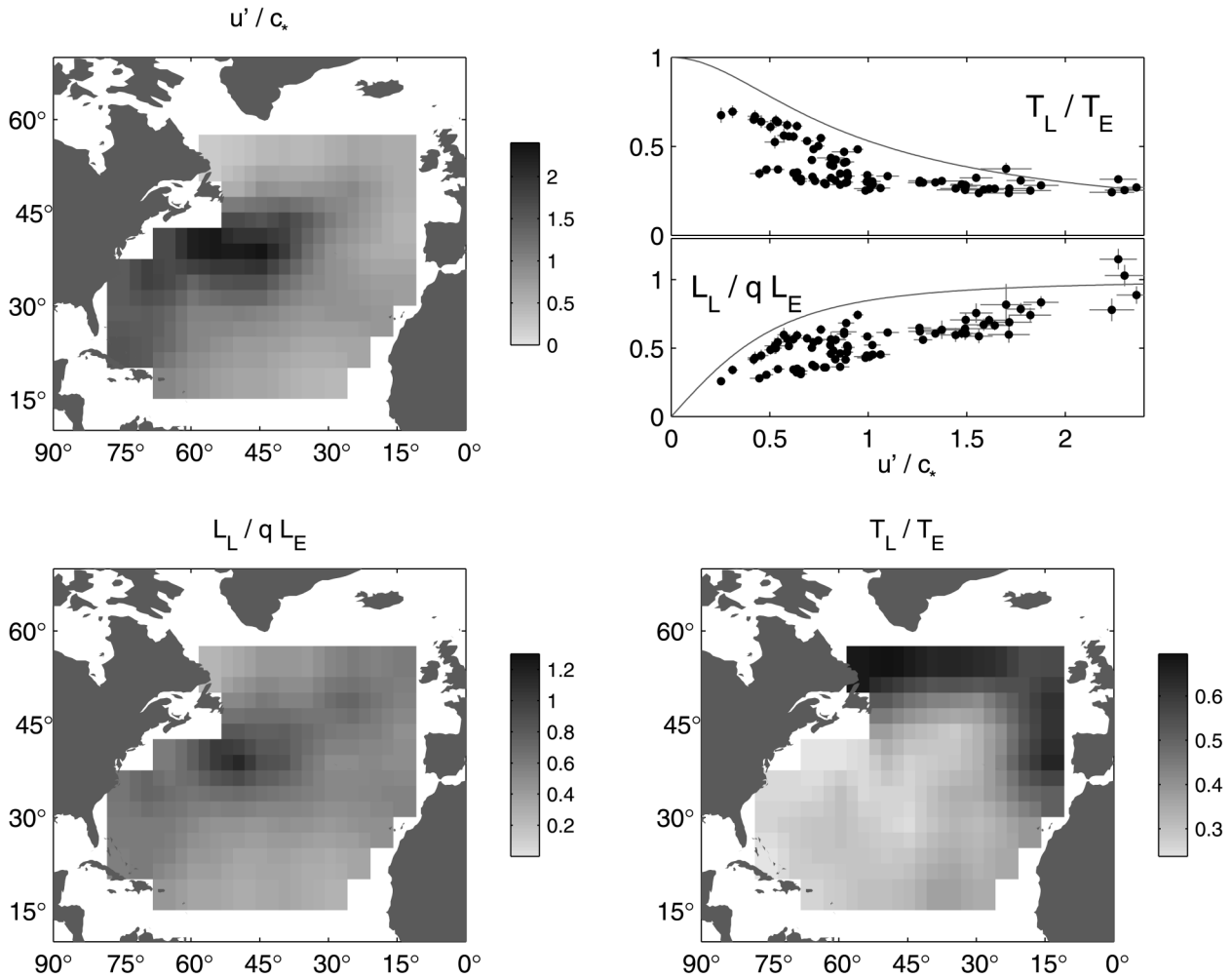
FIG. 9. A comparison of Lagrangian and Eulerian scales at the ocean surface. Eulerian scales are from Stammer (1997) (his Figs. 18b and 21a), averaged in 10° cells. Top, left: Distribution of u'/c_* (u' from surface drifters). Top, right: T_L/T_E (upper) and L_L/qL_E (lower), $q = \sqrt{\pi/8}$, as a function of u'/c_*. Bottom, left: Distribution of L_L/qL_E. Bottom, right: Distribution of T_L/T_E.

tions of Davis (1991), who showed that the Eulerian timescale has a strong influence on eddy diffusivity for small u'/c_*, and that L_E and u' determine κ_H only for large u'/c_*.

c. Implications for mesoscale linearity

Davis (1985) noted that the ratio T_L/T_E varied from unity for deep MODE floats to ∼0.3 for surface drifters in CODE. He attributed this to the significance of the advection terms in the Eulerian acceleration, with $T_L/T_E \sim 1$, $L_L \ll L_E$ in a nearly linear field of Rossby waves and $T_L \ll T_E$ in a fully nonlinear, turbulent field. In this context, Böning (1988) interpreted the sharp decrease in L_L from 700 m to 1500 m (see Fig. 3) as indicating a transition from a turbulent thermocline to a more wavelike subthermocline. However, although $T_L \sim T_E$ at 1500 m in MODE, the nonlinearity u'/c (where c is the phase propagation speed) was close to unity (Freeland et al. 1975).

To resolve this apparent discrepancy, note that linearity (small u'/c) is sufficient to produce fixed-float sampling (small u'/c_*, $c_* = L_E/T_E$), but it is not necessary. An eddy field may evolve more rapidly than L_E/c at a fixed point due to nonlinear interactions—c_* can be significantly larger than c. This happens in the deep layer of the CLIPPER model, where $c/c_* < 1/2$ outside the equatorial band (Fig. 10), allowing $u'/c_* < 1/2$ and $u'/c \sim O(1)$ over much of the subtropics. Thus, a field of nonlinear, turbulent vortices can produce the fixed-float sampling regime.

8. Concluding remarks

It is the Lagrangian, not Eulerian, scales that set absolute dispersion and give the associated eddy diffusivity. If oceanic floats uniformly encountered fixed-float ($T_L \sim T_E$, $L_L \propto u'$) or frozen-field ($T_L \propto 1/u'$, $L_L \propto L_E$) sampling conditions, then one could use $\kappa_H = u'^2 T_E$ or $\kappa_H = u'L_E$ (respectively) to calculate meaningful dif-
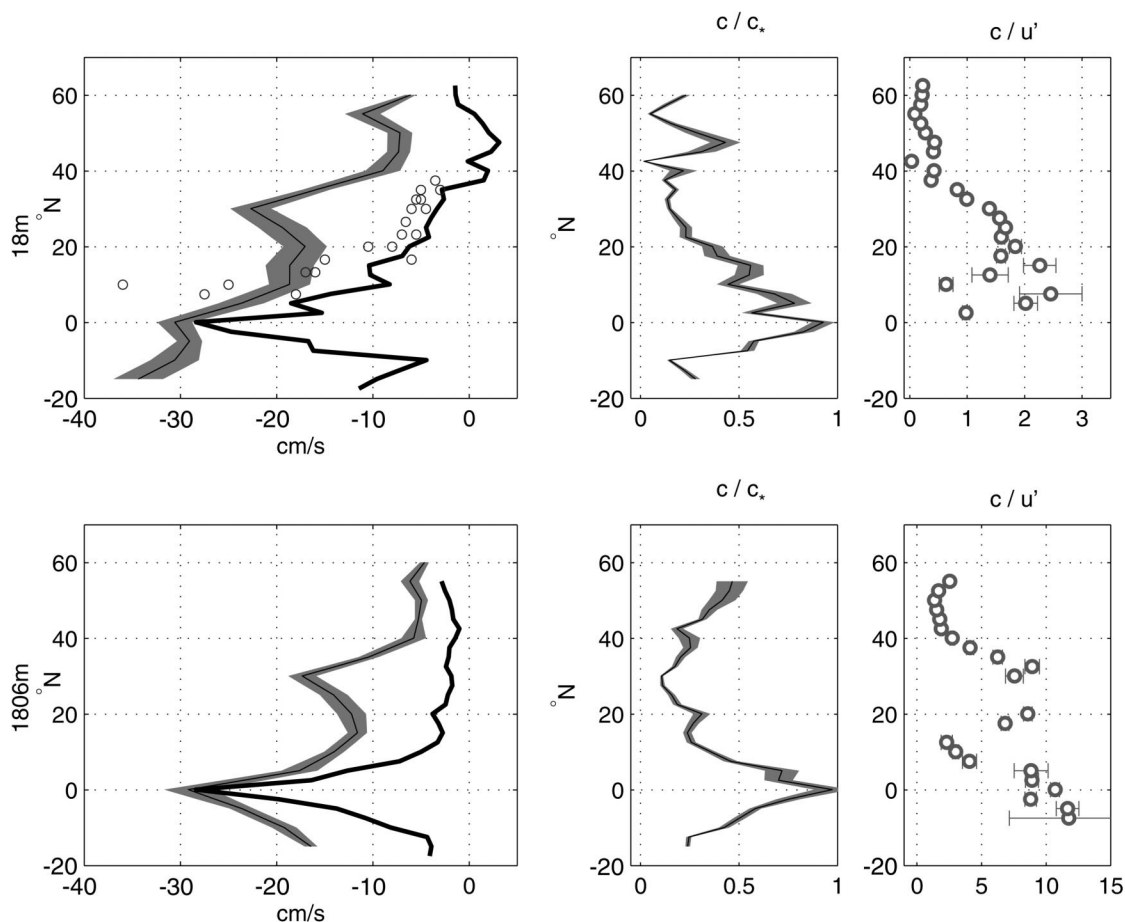
FIG. 10. Left: zonally averaged (0°–60°W) evolution speed $c_* = L_E/T_E$ (shaded error bar) in the model surface (top) and deep (bottom) layers. The westward drift speeds c of mesoscale fluctuations are also shown (heavy lines), calculated from Hovmöller diagrams (eddy energy as a function of longitude, 0–60°W, and time) averaging 2° of latitude. For reference, circles give propagation speeds derived from altimetry (Chelton and Schlax 1996). Middle: Ratio of propagation speed c to evolution speed c_* in the model. Right: ratio of propagation speed c to rms eddy speed u' in the model.

fusivities directly from Eulerian observations. However, our comparison of Lagrangian and Eulerian scales suggests that the ocean's sampling regime ranges from fixed-float to frozen-field—simple Eulerian-based recipes for κ_H are of dubious value.

In subregions of the ocean where the Eulerian scales are approximately constant and the sampling regime is uniformly fixed-float or frozen-field, a constant T_L or L_L can be anticipated. One example is the upper water column in the Gulf Stream: between the surface and 700 m, u' drops by 1.8 times while T_L increases by 1.6 times and L_L ($=u'T_L$) remains nearly constant, behavior consistent with frozen-field sampling conditions and $L_E \sim L_L/q \approx 100$ km. In this region of the upper ocean, such conditions would produce a diffusivity of $\kappa_H = (100$ km$)u'$, which can be mapped directly from Eulerian observations of surface EKE (cf. Stammer 1998).

Perhaps the most striking result of our study is the near-constant T_L in both the MODE and Eastern basin regions from depth 700 to 2000 m (Fig. 3), a feature

that could not be resolved in the absence of recent float observations (cf. Böning 1988). In these regions of the thermocline and subthermocline, one may use

$$\kappa_H \sim (6 \text{ days})u'^2 \tag{11}$$

to estimate a horizontal eddy diffusivity. This may be applicable to the deep ocean more generally, describing the dispersion for several multiples of T_L (e.g., the 120-day segments). If T_L is independent of u' due to fixed-float sampling in these regions, as we have suggested, then $T_L \sim T_E$ and the deep float observations map the distribution of T_E at far greater spatial resolution than provided by current meter moorings. Furthermore, a near-constant $T_E(z)$ suggests that the dynamics of the eddy field may not qualitatively change between the main thermocline and subthermocline, in contrast to the conclusions of Böning (1988). These conclusions need not imply that the deep interior eddy field is nearly linear: the field can be turbulent, that is, characterized
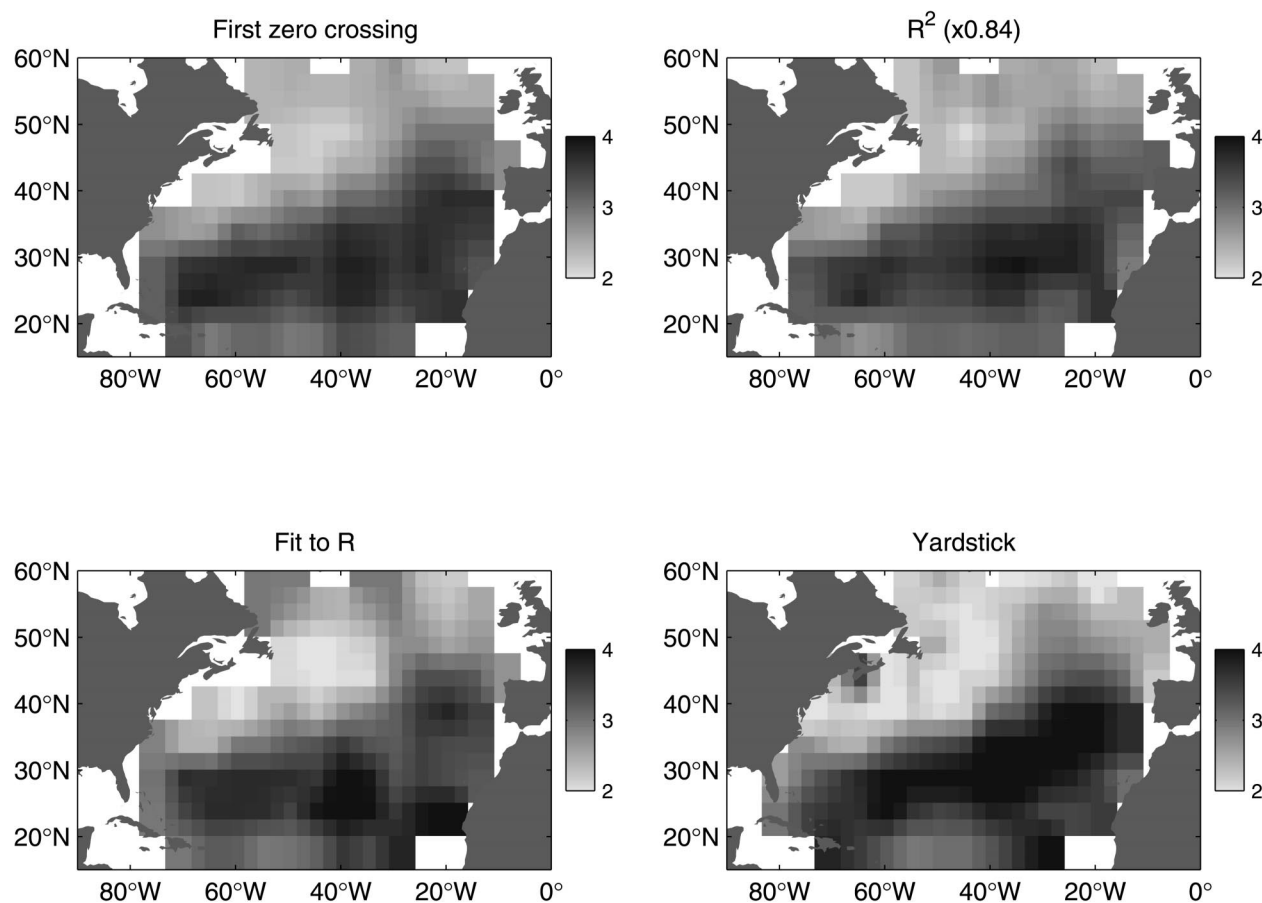
FIG. 11. The distribution of eddy timescale T_L (days) for the WOCE surface drifters, calculated by four different methods (see appendix A). Top, left: the observed autocorrelation function is integrated to the first zero crossing. Top, right: The squared autocorrelation function method (T_L multiplied by 0.84). Bottom, left: The prescribed autocorrelation function method. Bottom right: The yardstick method.

by $O(1)$ nonlinearity, and still produce fixed-float sampling conditions.

APPENDIX A

Alternative Methods for Calculating T_L

In practice, noise dominates the Lagrangian velocity autocorrelation function R at large lags. This introduces error when calculating T_L via (4) and integrating to the maximum record length. The most straightforward solution to this is to truncate the integral at some relatively short lag. Most researchers (cf. Freeland et al. 1975; Krauss and Böning 1987; Poulain and Niiler 1989) have chosen the decorrelation timescale T_D (the lag of first zero crossing of R), although some have chosen a constant lag (such as 20 d in Speer et al. 1999). If a constant lag is used, it must fall where noise-induced fluctuations dominate R, or the resulting T_L may depend on the physically meaningless value of the constant lag. For this reason, integration to T_D is more appropriate for large-scale studies where the decorrelation timescales can vary greatly.

In order to avoid truncating the integral in (4), several alternative methods have been proposed to estimate T_L. In this appendix, three of these methods are applied to the WOCE surface drifter trajectories, broken into 120-day segments and detrended. The resulting distribution of mean T_L (Fig. 11) shows that these alternative methods produce timescales consistent with those of the traditional method used here, indicating that this simplest

approach is a robust approximation to (4). We note, however, that this analysis does not explore the additional impact of low-frequency (periods much larger than 120 d) variations removed from the float trajectory segments.

Squared autocorrelation method. If the Lagrangian velocity consists of a pure sine wave of period P, integration to T_D produces $T_L = P/2\pi$. Without this truncation, (4) would fluctuate between $P/2\pi$ and zero, depending on the record length. Richman et al. (1977) argued that a pure sine wave should produce an infinite timescale, as it indicates a single process determines $u(t)$. This led them to propose an alternative definition for T_L,

$$T_L = \int_0^\infty d\tau R^2(\tau). \tag{A1}$$

As noted by Richman et al., this definition tends to produce longer timescales than (4), even with truncation at T_D. This method has a distinct disadvantage: noise-induced fluctuations tend to cancel when integrated over R, but always increase T_L in an integral over R^2. Thus, (A1) will produce T_L that are a function of record length if the noise-induced component of (A1) is significant compared to the signal-induced component.

For the drifters, this method produces T_L, which are on average 1.2 times greater than those presented here. Taking this factor into account, the two calculations yield similar maps of T_L.

Fitting a prescribed autocorrelation function. In their calculation of T_L from drifter data, Garraffo et al. (2001) fit an autocorrelation function of the form

$$R^*(\tau) = \cos\left(\frac{\pi\tau}{2T_D}\right)e^{-(\tau/\tau_e)^2} \tag{A2}$$

to the observed R, using the first zero crossing of R to set T_D and determining the e-folding timescale τ_e via a least squares fit. They used the exact integral of this function to infinite lag to get T_L:

$$T_L = \int_0^\infty d\tau R^*(\tau) = \frac{\sqrt{\pi}}{2}\tau_e e^{-(\pi\tau_e/4T_D)^2}. \tag{A3}$$

The traditional method of calculating T_L gives $T_L \sim T_D/2$. For fixed T_D, (A3) reaches a maximum for $\tau_e/T_D = 2\sqrt{2}/\pi \approx 0.9$, for which $T_L = \sqrt{2/\pi}e^{-1/2}T_D \approx 0.48T_D$. Smaller τ_e cause R^* to have an extremely narrow positive lobe, while larger τ_e produce deeper negative lobes; both effects reduce T_L.

For the average WOCE drifter, $\tau_e \sim 0.89T_D$ and the overall mean of T_L is 1.02 times larger than T_L from the traditional calculation. In the subtropics, $\tau_e/T_D \sim 1.2$–1.3, reflecting the presence of a stronger negative lobe in R, perhaps due to more wavelike dynamics at these latitudes. The effect on T_L is subtle: south of 30°N, it is smaller than in the traditional calculation by only 1.03

times. Thus, the map of surface T_L in Garraffo et al. (2001) strongly resembles the map of Fig. 4.

Yardstick method. Rupolo et al. (1996) proposed a unique method for calculating T_L that completely avoids integrating an autocorrelation function. In their method, a drifter trajectory's length is measured by a "yardstick" of fixed length Δ in a frame of reference moving at the mean drifter speed. The resulting measurement, $L(\Delta)$, is always smaller than $L(\Delta = 0)$ because of smoothing at scales smaller than Δ. When Δ is much larger than the eddy length scale, decreasing Δ causes a relatively fast increase in $L(\Delta)$. However, as Δ approaches the eddy length scale, the yardstick is applied over a distance for which u remains correlated with itself, so the measured trajectory length $L(\Delta)$ asymptotically approaches the constant value $L(0)$. The transition between the fractal behavior of $L(\Delta)$ at $\Delta \gg L_L$ and $L(\Delta) \sim L(0)$ at $\Delta \lesssim L_L$ thus gives an estimate of the eddy length scale. The yardstick length scale L_{yard} can be defined as

$$L(L_{\text{yard}}) = \frac{2}{\pi}L(0), \tag{A4}$$

so a perfectly circular drifter trajectory of diameter D will have $L_{\text{yard}} = D$. The integral timescale can then be defined as

$$T_L = \mu L_{\text{yard}}/u', \tag{A5}$$

where the constant μ is chosen to produce mean scales consistent with (4) (Rupolo et al. 1996). For the surface drifters, we find $\mu = 0.40$. The yardstick method produces T_L that span a wider range of values than via the traditional method: subtropical maxima are $\sim$1.05 times larger, while subpolar minima are $\sim$1.1 times smaller. Qualitatively, the distribution of yardstick-derived T_L is similar to that of the traditional method.

APPENDIX B

Sources of Error

The ratio of Lagrangian to Eulerian scales in the model tend to obey (9) and (10), but with considerable scatter for the 10° averages. Sources of this scatter include:

Violation of the theory's assumptions. Middleton's theory assumes the motion is nondivergent, which is not the case for floats constrained to a constant-pressure layer in the simulated or actual ocean. The theory also assumes that the Eulerian statistics are stationary and homogeneous. In the model, as in the actual ocean, eddy energy and scales change in space and time. We have attempted to minimize these effects via 10° cell averages, but cannot eliminate them entirely. For example, float trajectories have been broken into 120-day segments in this study. Had a shorter duration been chosen, the trajectories would be shorter and thus less sensitive to large-scale inhomogeneities. However, the energy-containing eddy band is $\sim$50–150 day in Eulerian spectra (Richman et al. 1977), and thus should be at similar

periods in fixed-float Lagrangian spectra. Because the eddy band is red, shorter time series can produce shorter timescales that are a function of the record length. Thus, comparing Eulerian and Lagrangian scales in the ocean will inevitably require a balance between neglecting the red end of the eddy spectrum (producing artificially shortened timescales, especially in the fixed-float regime) and introducing errors due to inhomogeneity.

Measurement error. Eddy scales calculated from a finite time series are only approximations to the true integral scales, for which Middleton (1985) applies (see appendix A). The overall distribution of the eddy scales is not strongly sensitive to this approximation, but values in individual $10°$ cells can vary considerably. Thus, the finite-time approximation to (4) introduces some scatter to the eddy scales.

Theoretical inaccuracy. As noted by Middleton, Corrsin's conjecture (Corrsin 1959) is accurate only when the Eulerian and Lagrangian timescales are of the same order. Thus, the theory (which relies on this conjecture) may be systematically incorrect in the limit $u'/c_* \gg 1$. Such behavior is not apparent in the $\frac{1}{3}°$ model (Fig. 8), but this may be due to the limited range of u'/c_*. Higher resolution models will be able to resolve this issue in future studies.

Doppler-shifting of the Eulerian timescale. Relation (9) assumes that the eddy field is not moving. However, oceanic mesoscale features drift westward (Chelton and Schlax 1996) due to β-induced free propagation, with variations from linear theory caused by advection by mean currents, alteration of the local planetary vorticity by mean shear, the superposition of forced waves, and a host of other possible mechanisms (cf. Qiu et al. 1997; Dewar 1998). This drift can shorten the apparent timescale for fixed observers. For example, consider the extreme case of an unchanging (frozen) field drifting at speed c: the Eulerian timescale is $T_E = L_E/c$, but in the reference frame moving at c the apparent Eulerian timescale (for which Middleton's relationships are formulated) is $T'_E = \infty$. If the mesoscale field is evolving, T'_E is finite and T_E satisfies $T_E < L_E/c$. Middleton (1985) suggested a relationship of the form

$$T'_E \sim T_E \left[1 - \left(\frac{c}{c_*} \right)^2 \right]^{-1/2}, \qquad (B1)$$

which satisfies $T'_E \to \infty$ for $T_E \to L_E/c$ and $T'_E \to T_E$ for $c/c_* \to 0$. In the surface model layer, mesoscale disturbances drift westward at speeds close to the first baroclinic Rossby wave speed (Fig. 10) (the model does not appear to replicate the discrepancy with linear theory noted by Chelton and Schlax 1996). Except near the model's equator, c is generally much smaller than the evolution speed c_*; thus, eddy fluctuations look similar in the fixed, Eulerian frame and in a frame moving at c. Few $10°$ cells have $|c/c_*|^2 > 0.2$, suggesting that Doppler-shifting is not a major source of scatter.

Scatter inherent in the theory. Middleton derived (9)

for a particular Eulerian field, but found that the ratio T_L/T_E as a function of u'/c_* varied by $\sim 10\%$ for widely ranging Eulerian statistics. Because the model Eulerian field has spatially varying length and timescales, similar scatter could appear in Fig. 8 without appealing to any of the previous arguments.

REFERENCES

Batchelor, G. K., 1949: Diffusion in a field of homogeneous turbulence: I. Eulerian analysis. *Aust. J. Sci. Res.,* **2A,** 437–450.

Blanke, B., and S. Raynaud, 1997: Kinematics of the Pacific Equatorial Undercurrent: An Eulerian and Lagrangian approach from GCM results. *J. Phys. Oceanogr.,* **37,** 1038–1053.

Böning, C., 1988: Characteristics of particle dispersion in the North Atlantic: An alternative interpretation of SOFAR float results. *Deep-Sea Res.,* **35,** 1379–1385.

Brink, K., R. Beardsley, P. Niiler, M. Abbott, A. Huyer, S. Ramp, T. Stanton, and D. Stuart, 1991: Statistical properties of near-surface flow in the California coastal transition zone. *J. Geophys. Res.,* **96,** 14 693–14 706.

Chelton, D. B., and M. Schlax, 1996: Global observations of oceanic Rossby waves. *Science,* **272,** 234–238.

Corrsin, S., 1959: Progress report on some turbulent diffusion research. *Advances in Geophysics,* Vol. 6, Academic Press, 161–162.

Davis, R., 1982: On relating Eulerian and Lagrangian velocity statistics: Single particles in homogeneous flows. *J. Fluid Mech.,* **114,** 1–26.

——, 1985: Drifter observations of coastal surface currents during CODE: The statistical and dynamical views. *J. Geophys. Res.,* **90,** 4756–4772.

——, 1991: Observing the general circulation with floats. *Deep-Sea Res.,* **38,** S531–S571.

Dewar, W., 1998: On "too fast" baroclinic planetary waves in the general circulation. *J. Phys. Oceanogr.,* **28,** 1739–1758.

Fratantoni, D. M., 2001: North Atlantic surface circulation during the 1990's observed with satellite-tracked drifters. *J. Geophys. Res.,* **106,** 22 067–22 093.

Freeland, H., P. Rhines, and T. Rossby, 1975: Statistical observations of the trajectories of neutrally buoyant floats in the North Atlantic. *J. Mar. Res.,* **33,** 383–404.

Garraffo, Z., A. J. Mariano, A. Griffa, C. Veneziani, and E. Chassignet, 2001: Lagrangian data in a high resolution numerical simulation of the North Atlantic. I: Comparison with in situ drifter data. *J. Mar. Syst.,* **29,** 157–176.

Garrett, C., 1994: Dispersion and mixing in the ocean. *Ocean Processes in Climate Dynamics: Global and Mediterranean Examples,* P. Malanotte-Rizzoli and A. R. Robinson, Eds., Kluwer Academic, 61–77.

Hansen, D., and P.-M. Poulain, 1996: Quality control and interpolations of WOCE–TOGA drifter data. *J. Atmos. Oceanic Technol.,* **13,** 900–909.

Hua, B.-L., J. McWilliams, and P. Klein, 1998: Lagrangian accelerations in geostrophic turbulence. *J. Fluid Mech.,* **366,** 87–108.

Krauss, W., and C. Böning, 1987: Lagrangian properties of eddy fields in the northern North Atlantic as deduced from satellite-tracked buoys. *J. Mar. Res.,* **45,** 259–291.

Lumpkin, R., and P. Flament, 2001: Lagrangian statistics in the central North Pacific. *J. Mar. Syst.,* **29,** 141–155.

McWilliams, J., and Coauthors, 1983: The local dynamics of eddies in the western North Atlantic. *Eddies in Marine Science,* A. Robinson, Ed., Springer-Verlag, 92–113.

Middleton, J., 1985: Drifter spectra and diffusivities. *J. Mar. Res.,* **43,** 37–55.

Niiler, P., R. Davis, and H. White, 1987: Water-following characteristics of a mixed-layer drifter. *Deep-Sea Res.,* **34,** 1867–1882.

O'Dwyer, J., R. G Williams, J. LaCasce, and K. Speer, 2000: Does

the potential vorticity distribution constrain the spreading of floats in the North Atlantic? *J. Phys. Oceanogr.,* **30,** 721–732.

Owens, W. B., 1991: A statistical description of the mean circulation and eddy variability in the northwestern Atlantic using SOFAR floats. *Progress in Oceanography,* Vol. 28, Pergamon, 257–303.

Poulain, P.-M., and P. Niiler, 1989: Statistical analysis of the surface circulation in the California Current System using satellite-tracked drifters. *J. Phys. Oceanogr.,* **19,** 1588–1603.

Qiu, B., W. Mao, and P. Müller, 1997: Propagation and decay of forced and free baroclinic Rossby waves in off-equatorial oceans. *J. Phys. Oceanogr.,* **27,** 2405–2417.

Richman, J., C. Wunsch, and N. Hogg, 1977: Space and time scales of mesoscale motion in the western North Atlantic. *Rev. Geophys. Space Phys.,* **15,** 385–420.

Rossby, H., S. Riser, and A. Mariano, 1983: The western North Atlantic—a Lagrangian view-point. *Eddies in Marine Science,* A. Robinson, Ed., Springer-Verlag, 66–91.

Rupolo, V., B.-L. Hua, A. Provenzale, and V. Artale, 1996: Lagrangian velocity spectra at 700 m in the western North Atlantic. *J. Phys. Oceanogr.,* **26,** 1591–1607.

Speer, K., J. Gould, and J. LaCasce, 1999: Year-long float trajectories in the Labrador Sea Water of the eastern North Atlantic. *Deep-Sea Res.,* **46,** 165–179.

Stammer, D., 1997: Global characteristics of ocean variability estimated from regional TOPEX/Poseidon altimeter measurements. *J. Phys. Oceanogr.,* **27,** 1743–1769.

——, 1998: On eddy characteristics, eddy transports, and mean flow properties. *J. Phys. Oceanogr.,* **28,** 727–739.

——, and C. Böning, 1992: Mesoscale variability in the Atlantic Ocean from Geosat altimetry and WOCE high-resolution numerical modeling. *J. Phys. Oceanogr.,* **22,** 732–752.

Swenson, M., and P. Niiler, 1996: Statistical analysis of the surface circulation of the California Current. *J. Geophys. Res.,* **101,** 22 631–22 645.

Taylor, G., 1921: Diffusion by continuous movements. *Proc. London Math. Soc.,* **20,** 196–212.

Treguier, A.-M., and Coauthors, 1999: The CLIPPER project: High resolution modelling of the Atlantic. *International WOCE Newsletter,* No. 36, WOCE International Project Office, Southhampton, United Kingdom, 3–5.

——, and Coauthors, 2001: An eddy permitting model of the Atlantic circulation: Evaluating open boundary conditions. *J. Geophys. Res.,* **106,** 22 115–22 129.